

# Spontaneous vortex phases in ferromagnet-superconductor nanocomposites

Y. T. Xing<sup>1</sup>, H. Micklitz<sup>1</sup>, T. G. Rappoport<sup>2</sup>, M. V. Milošević<sup>3</sup>, I. G. Solórzano-Naranjo<sup>4</sup>, and E. Baggio-Saitovitch<sup>1</sup>

<sup>1</sup>*Centro Brasileiro de Pesquisas Físicas, Rio de Janeiro 22290-180, Brazil*

<sup>2</sup>*Instituto de Física, Universidade Federal do Rio de Janeiro,  
Cx. P. 68528, 219s41-972, Rio de Janeiro, Brazil*

<sup>3</sup>*Departement Fysica, Universiteit Antwerpen,*

*Groenenborgerlaan 171, B-2020 Antwerpen, Belgium and*

<sup>4</sup>*DCMM, Pontifícia Universidade Católica do Rio de Janeiro,  
Cx. P. 38071, 22453-970, Rio de Janeiro, Brazil*

We report the appearance of spontaneous vortices in lead superconducting films with embedded magnetic nanoparticles and a temperature induced phase transition between different vortex phases. Unlike common vortices in superconductors, the vortex phase appears in the absence of applied magnetic field. The vortices nucleate exclusively due to the stray field of the magnetic nanoparticles, which serve the dual role of providing the internal field and simultaneously acting as pinning centers. Transport measurements reveal dynamical phase transitions that depend on temperature (T) and applied field (H) and support the obtained (H-T) phase diagram.

PACS numbers: 74.25.Dw, 74.25.Fy, 74.81.Bd

The interplay between of superconductivity (SC) and ferromagnetism (FM) has been attracting the attention of the scientific community since the discovery of superconductivity [1]. Recently, there has been a resurgence of this interest due to new phenomena: for example, the increase of the critical current  $J_c$  in hybrid systems containing sub-micron ferromagnetic particles on top of type II superconductors [2, 3] and the coexistence of superconductivity with long-range magnetic order in magnetic superconductors [4]. In a SC-FM hybrid, the magnets strongly affect the properties of the superconductor, leading to a change in the critical temperature  $T_c$  and critical current  $J_c$ . Also, they give an opportunity to observe new phenomena such as domain-wall superconductivity[5] and hysteresis pinning effect[6].

In order to study the characteristics of the novel spontaneous vortex phases that arise from the interaction between vortices and embedded magnetic nanoparticles, we fabricated a hybrid system that consists of a 100 nm lead film (Pb) containing homogeneously distributed single domain cobalt (Co) particles (mean diameter about 4.5 nm) with randomly oriented magnetization.

The samples are produced by the so-called inert-gas(Ar) aggregation method with an Ar pressure of about  $10^{-1}$  mbar. It is a co-deposition of Pb and well-defined Co clusters directly onto a sapphire substrate without buffer and capping layer. The Ar is absorbed by a cryopump at the other end of the cluster chamber and only well-defined Co clusters can enter the main chamber. The substrate is mounted on a coldfinger of a rotatable <sup>4</sup>He cryostat and is cooled to  $\sim 40$  K during the deposition. The samples are deposited at low temperature in order to get high quality Pb films. The angle between the matrix and the cluster beams was  $45^\circ$ . Due to the different beam directions, samples with different Co volume fraction can be made within one preparation. The de-

position rates are controlled by three quartz balances in order to monitor the deposition rate at different positions of the substrate. Ag contacts for transport measurements are pre-deposited and connected to a multi-channel automatic measurement system. The typical dimensions of the sample were  $10\text{mm}\times 3\text{mm}\times 100\text{nm}$ . After deposition, transport properties in both zero and non-zero magnetic field were investigated in-situ with a built-in split-coil superconducting magnet ( $B \leq 1.2\text{T}$ ).

This method has some advantages: first, the size of the Co nanoparticles is tunable and its distribution is very narrow, with a standard deviation of less than 1nm. Second, due to the fact that we do not use any buffer or capping layer, any measurement is related exclusively to the Pb-Co sample. Third, the magnetic moments of the Co particles are randomly oriented so that they have zero total magnetic moment in the sample. After deposition, the samples were annealed at 300 K in order to decrease the defect density. The sample of Co clusters for the microstructure study was deposited on a carbon foil which was mounted on a TEM-catcher. A more detailed description of the experimental set-up and operating procedures for the same equipment and a similar system of Ag matrix and Co particles can be found in the literature [7].

The morphology of the Co nanoparticles was inferred by transmission electron microscopy (TEM). As displayed in Fig. 1 (a), they are very homogeneous in shape with a mean diameter of  $d\sim 4.5$  nm, therefore smaller than the vortex core size (see below). Fig. 1(b) charts a typical magnetic hysteresis loop measured with a SQUID at a temperature just above  $T_c$ , indicating that the Co clusters are indeed ferromagnetic. Similar nanocomposites have been produced previously [6, 8, 9]. However, the appearance of vortices in these systems in the absence of applied magnetic field has never been observed before.

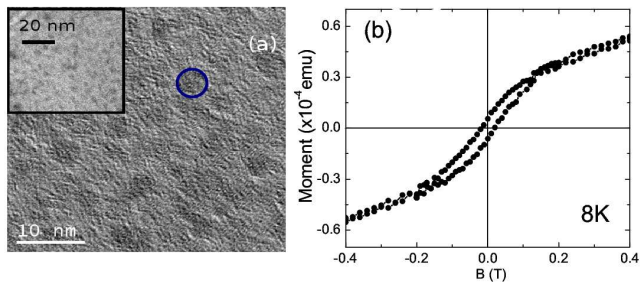


FIG. 1: (Color online) (a) TEM image of the Co nanoclusters. (b) Hysteresis loop for a sample with 5% Co volume fraction at 8K.

The nanocomposites were mainly used to investigate the pinning effect of magnetic nanoparticles in the superconducting phase in the presence of an external magnetic field.

Theoretical calculations predict that due to their stray field, ferromagnets inside a superconductor can lead to flux bundles in the form of spontaneous vortices, antivortices, loops and even closed loops [10, 11]. In contrast with other systems in which superconductivity and ferromagnetism coexist [4, 5], the ferromagnetic constituents in the present case are small single domain particles with randomly oriented magnetization. Both the size of the particles and the mean distance between them are smaller than the coherence length ( $\xi$ ) and penetration depth ( $\lambda$ ). The Co clusters have considerable magnetic moments and thus a strong magnetic stray field. If the diameter of the particle (4.5 nm) is much smaller than  $\lambda \sim 80$  nm, the difference of the stray field between a free magnetic particle and a particle in a superconductor is less than one percent. It means the effect of the superconductivity on the stray field of Co particles can be ignored in our case. The maximum field strength of this stray field for a single domain Co particle is about 1.3 T at the poles (corresponding to the Co bulk saturation magnetization of about 1.8 T) and, therefore, much larger than the critical field of  $B_c(0) = 0.1$  T for pure Pb. This fact together with the well-known suppression of superconductivity due to the proximity effect caused by non-superconducting metallic particles embedded in a superconductor (eg. Cu particles in Pb [12]) makes a favorable scenario for the formation of spontaneous vortices inside the superconducting Pb film.

Transport measurements give a signature of the presence of vortices in a SC and thus can be used to characterize a vortex state. In order to probe the nucleation of the spontaneous vortices in our films, we analyze the temperature (T) dependence of the resistivity ( $\rho$ ).

In Fig. 2, the  $\rho$ -T curves of different samples are shown. Fig. 2 (a) gives the  $\rho$ -T curves for an as-prepared film (deposition temperature: 40K) with a Co concentration of 3.7 v%. One can see a sharp transition at a critical temperature  $T_c \sim 5.5$  K. Compared to  $T_c \sim 7.2$  K of an

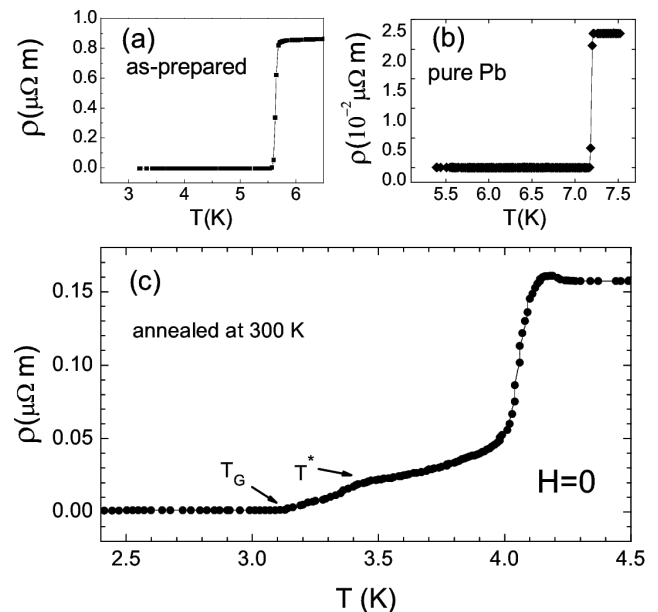


FIG. 2: Resistivity ( $\rho$ ) versus temperature (T) for (a) an as-prepared film of lead containing about 3.7 v% cobalt nanoparticles at zero applied magnetic field, (b) a reference sample of pure lead prepared by the same method and (c) the same sample in (a) but annealed at 300 K.  $T_G$  is the temperature that characterizes the transition to a zero-resistance state.  $T^*$  is a temperature that indicates the kink in the resistivity. The current used in all measurements was  $I = 0.1$  mA.

undoped pure Pb film, deposited at 40 K and annealed at 300K (Fig. 2 (b)), the Co-doped sample has the expected reduction  $T_c$  caused by the two effects discussed above, namely, the proximity effect and the formation of spontaneous vortices. If we compare our  $T_c$  reduction ( $\Delta T_c \sim 1.7$  K or  $\approx 0.5$  K/v%Co) with that found in granular Cu/Pb structures [12] where the  $T_c$  reduction is due to the proximity effect only ( $\Delta T_c \sim 0.12$  K/v%Cu), we can conclude that the effect of spontaneous vortex formation in our Pb/Co system probably is the dominating effect in the  $T_c$  reduction. If should be mentioned, however, that this reduction in  $T_c$  due to 3.7 v% Co clusters is much smaller than that caused by Co atoms in Pb [13]. There a decrease of 2 K/v% Co is observed, which is caused by pair-breaking due to spin flip scattering at paramagnetic impurities. In the case of our Co clusters, having a superparamagnetic blocking temperature of  $\sim 25$  K, such a process can not occur below  $T_c$ .

Annealing the sample at 300 K has dramatic effects (see Fig 2 (c)): it not only reduces the resistivity in the normal state by a factor of  $\sim 5$ , but also changes the superconducting transition. Besides a further reduction of  $T_c$ , a strongly broadened and structured transition is observed, having zero resistivity at low temperature but an ohmic region between 3.1 and 3.6 K which is followed by a small kink and a second increase of the of the resistivity below the main transition to the normal state at about 4 K. It

is important to point out that although the main feature of the  $\rho$ - $T$  curves for several studied sample are similar, their exact form and the characteristic temperatures depends on the Co volume fraction [14].

In the following we will discuss in detail the structure in the  $\rho$ - $T$  curve of the annealed sample shown in Fig. 2. From the resistivity of the annealed sample we can estimate the superconducting coherence length  $\xi$  of this sample. Since the upper critical field  $H_{c2}$  in our case is given by a sum of external applied field and the stray field of the Co particles, we avoid estimating the coherence length  $\xi$  from  $H_{c2}$ . Instead we assume the dirty limit for type II SCs and get the mean-free path from the normal state resistivity (see Fig. 2 (c)) to determine the coherence length from the following expression:

$$\xi = 0.855(\xi_0 l)^{1/2} \sqrt{1 - \frac{T}{T_c}} \quad (1)$$

where  $\xi_0 = 83$  nm is the coherence length of pure lead at zero temperature and  $l$  is the mean-free path. The values of  $l$  were obtained from the resistivity using the free electron model. The sample mean-free path is  $l = 3.1$  nm leading to an estimated  $\xi \sim 25$  nm for temperatures close to 3 K. As discussed above, the ratio between  $\xi$  and  $\lambda$  indicates that the sample is a type II superconductor. The anomalous  $\rho$ - $T$  curve for  $H = 0$  is a first indication of the existence of more than one phase of vortices or other forms of trapped flux inside the superconductor. Close to the critical temperature, we also see a resistance anomaly that is absent in the non-annealed samples and it is destroyed by magnetic field. It is known that similar excess resistances were reported in superconducting Al nanostructures [15, 16, 17] and inhomogeneous superconducting films [18]. Some possible origins for the phenomena are normal-superconducting (N-S) interfaces induced by dynamic phase slip centers [15, 16] or non-homogeneous distribution of critical temperatures inside the sample [17]. This anomaly was also reported in a system composed of a SC doped with magnetic impurities [19]. We do not know the exact reason for the appearance of the resistance peak in our sample. However, it is of no relevance for the feature in the  $\rho$ - $T$  curve far below the onset of the superconductivity.

This low temperature  $H = 0$  behavior we see in Fig. 2 (c) is similar to the one observed in type II SCs, such as Y-Ba-Cu-O containing random point defects [20] or amorphous SCs such as MoSi [21] under an applied magnetic field. The curves suggest that at very low temperatures the vortices are organized in a solid state phase. Due to the random orientation of the magnetic particles and presence of loops, we presume that the vortices are highly entangled leading to a kind of vortex glass. Above 3.1 K, the onset of the ohmic behavior corresponds to a phase transition with thermally induced vortex movement. The kink at  $T^*$  represents a transition between liquids in different pinning regimes or the rearrangement

and breaking of the vortex loops without depinning from the pinning centers. However, from these measurements, it is difficult to characterize the phases. We could attribute this resistivity behavior to either a spontaneous creation of vortices that connect to the sample boundaries, some other type of trapped vortex state [10] or flux creep [22].

The most convincing evidence of the existence of a spontaneous vortex solid (SVS) at low temperatures comes from the characterization of the vortex dynamics by means of isothermal voltage (V)-current (I) measurements. Fig. 3(a) and Fig. 3(b) show a set of (V-I) curves for the same sample of Fig. 2 at  $H = 0$  and temperatures ranging from 2.26 K to 4.2 K. They indicate the existence of spontaneous vortices networks or loops induced solely by the magnetic nanoparticles' stray field. For a better understanding of the relation between the  $\rho$ - $T$  and (V-I) curves, we focus on the curves below the main transition (Fig. 3(b)): for low temperatures, the voltage is zero for low currents, which indicates the existence of a vortex solid. Furthermore, it increases exponentially with increasing current, a characteristic of both vortex glass and flux creep [23]. For intermediate temperatures, the V-I curves have an S-shape, associated to vortex movements with two different activation energies. Finally, it increases monotonically with current for temperatures just below  $T_c$ , as it is expected for a normal vortex liquid.

On a logarithmic scale (Fig. 3(a)) a simpler picture appears, with a clear separation of two classes of (V-I) curves: one for low temperatures, below a critical line  $T_G$  and the other for high temperatures. The (V-I) curves show a positive curvature for higher T and an ohmic behavior for low currents while for low T the curves have a negative curvature. The onset of ohmic behavior corresponds to a liquid phase and the exponential decrease of the voltage for decreasing values of the current is the signature of a vortex glass phase [24].

In order to gain a better understanding of the dynamic response of this vortex structure, we use a scaling theory in the critical region of a vortex-glass transition. In the scaling regime, the relation between the electrical field  $E$  and the current density  $J$  is given by

$$E|t|^{-\nu(z+2-D)} = F_{\pm}(|t|^{-(D-1)\nu} J), \quad (2)$$

where  $t = (T - T_G)/T_G$ ,  $T_G$  is the temperature for the vortex glass transition and  $F_{\pm}$  are two universal functions for  $t > 0$  and  $t < 0$  [23].  $D$  is the dimensionality of the phase transition,  $z$  is the dynamical exponent and  $\nu$  is the exponent related to the divergence of the coherence length ( $\xi \sim |T - T_G|^{-\nu}$ ). Using this scaling relation with  $D = 3$ ,  $T_G = 3.15$  K,  $\nu = 3/8$  and  $z = 2.73$ , the set of data from Fig. 3(a) ranging from 2.2 K to 3.8 K can be scaled to the same universal functions as shown in Fig. 3(c). This universality lends strong support to the presence of a second order phase transition. The values

of the exponents  $z$  and  $\nu$  are smaller but comparable to the exponents of the vortex glass transition obtained for Y-Ba-Cu-O containing random point defects [25] and for amorphous superconductors [21]. The difference in the exponents gives us a transition with smaller correlation lengths and relaxation rates.

In earlier experiments on embedded magnetic nanoparticles in SCs, an increase of vortex pinning due to the presence of the magnetic particles has been observed [8, 9, 26]. In general, these pinning centers are extremely efficient and can be originated by various physical effects [6, 8, 27, 28]. In our case, we have an even stronger constraint: the hybrid systems have an intrinsic pinning, since the magnetic particles produce the vortices and pin them to their original location. In this sense, the difference in the scaling exponents should be related with the different type of pinning centers created by magnetic nanoparticles. We believe that an extension of the scaling theory addressing the issue of magnetic pinning is needed in order to fully understand this new spontaneous vortex solid (SVS).

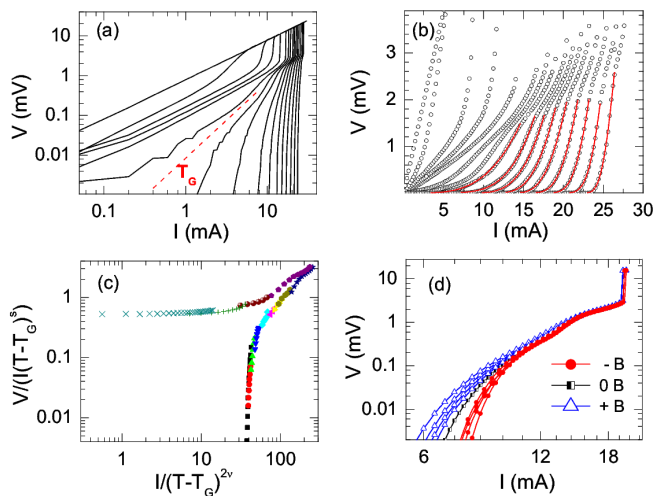


FIG. 3: (Color online) (a) Isotherms of voltage ( $V$ ) versus current ( $I$ ) in a log-log scale with no magnetic field applied and  $T$  are 2.26, 2.35, 2.44, 2.53, 2.6, 2.72, 2.8, 2.9, 3.0, 3.1, 3.2, 3.4, 3.6, 3.8, 4.0 and 4.2 K from right to left. (b) Low-voltage region of the same isotherms of  $V$ - $I$ . (c) Scaling analysis for the same data presented in (a) from  $T$  varying from 2.44K to 3.8K. The exponent  $s$  is given by  $s = \nu(z - 2 + D)$ . In the curves different colors indicate different temperatures. (d) Effect of positive and negative magnetic field (varying from -0.01 T to 0.01T) in the  $V$ - $I$  curves at 2.9 K. For details, see main text.

Now we also can understand the observed sharp superconducting transition of the as-prepared sample shown in of Fig. 2 (a): due to the low deposition temperature of 40 K, the non-annealed sample has a large number of defects which results: (i) in a high resistivity of the normal state, (ii) a reduction of the  $\xi$  ( $\xi \propto l^{1/2}$ ) and (iii) in strong vortex pinning. Due to the later one the spontaneous vortex

solid will remain up to the transition temperature  $T_c$  resulting in a sharp transition at  $T_c$ .

For a further investigation of how the nanoparticles' magnetization modifies the low temperature vortex state, we study the ( $V$ - $I$ ) curves for  $B$  up to 0.01 T, which is much smaller than the field necessary to align the magnetic particles (Fig. 1(b)). The magnetic field is applied parallel to the sample surface and we use the following procedure: we first align the nanoparticles at room temperature with a magnetic field  $B = 1$  T, in order to obtain a net stray field of the Co particles ( $B_{Co}$ ), i.e.  $B_{Co} \neq 0$ . Next, we field-cool the system and turn off the field at a temperature above  $T_c$  but far below the blocking temperature of the particles. We then apply the small magnetic field in opposite directions at fixed temperature below  $T_c$ . We find an asymmetric behavior of the ( $V$ - $I$ ) curves for different polarities of the field (Fig. 3(d)). This result can be seen as a superposition of two different effects. The relation of the total field ( $B_T$ ) inside the sample, the external field ( $B_{ext}$ ) and the field of the Co clusters is  $B_{T+} = B_{ext} + B_{Co}$  but with reversed external field the relation becomes  $B_{T-} = B_{ext} - B_{Co}$ . This difference gives rise to a very small shift in the critical current that depends on the field direction. A similar result was observed in other systems of nanomagnets inside a superconductor [6]. A novel and more pronounced effect occurs at small currents, when opposite fields play the role of moving the system toward the phases above or below the vortex glass transition.

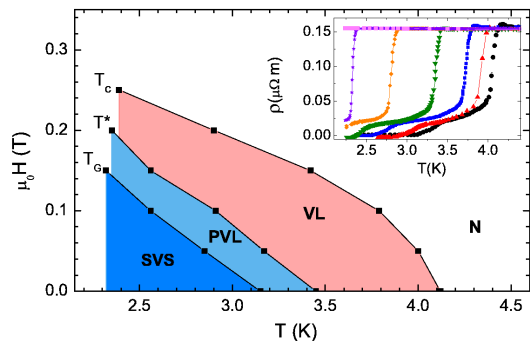


FIG. 4: (Color online)  $H$ - $T$  phase diagram of the hybrid system containing Co nanoparticles. SVS represents the spontaneous vortex solid. It is separated by critical line  $T_G$  from a strongly pinned vortex liquid (PVL). The boundary to the unpinned vortex liquid (VL) is  $T^*$ , the characteristic temperature of the kink feature seen in figure 2. The last critical curve is the main superconducting transition at  $T_c$  to the normal state (N). Inset: resistivity ( $\rho$ ) versus temperature ( $T$ ) for various applied magnetic fields from 0 T to 0.3 T (right to left).

For applied fields higher than the coercive field of the sample, the ( $V$ - $I$ ) curves do not depend on the polarity of the field. Therefore we analyze the ( $\rho$ - $T$ ) (inset of Fig 4) and ( $V$ - $I$ ) data in the presence of an external magnetic field and construct an  $H$ - $T$  phase diagram. As before, the



field is in-plane but now it is strong enough to increase the net stray field produced by the Co particles and the total field  $B_T$ . As can be seen in the diagram of Fig. 4, it suppresses the superconductivity, shifting the transitions ( $T_G$ ,  $T^*$  and  $T_c$ ) to lower temperatures. Together with the reduction of the critical temperatures, there is a shrink in the SVS phase, showing that the intrinsic pinning is stronger than the normal magnetic pinning. Finally, we can see that the lines  $T_G$  and  $T^*$  are parallel to each other. It could indicate that the pinned liquid state (PVL) is indeed a phase of partial movement, where the vortices disentangle with reorientation and break of loops [29]. This non-linear effect could also be a consequence of the inhomogeneous character of this superconducting phase and different nature of pinning centers (magnetic and nonmagnetic). This can constrain the vortex movement and also give rise to regions with different pinning strengths.

In conclusion, our transport measurements show the signature of novel spontaneous vortex phases in superconducting films with embedded magnetic particles. At low temperatures, the spontaneous vortices are organized in a disordered solid state (SVS), similar to a glass. For increasing temperatures, the system undergoes a second order phase transition to a pinned vortex liquid followed by a crossover that resembles vortex depinning. The dependence of the vortex solid state on the polarity of the magnetic field demonstrates that ferromagnetic particles inside superconductors can be used for specific forms of vortex creation and manipulation.

This work was partially supported by CAPES/DAAD cooperation program and the Brazilian agencies CNPq, FAPERJ (Cientistas do Nosso Estado and PRONEX) and L'Oreal Brazil. T. G. R and M. V. M would like to thank ITS at UND for the hospitality. H. M acknowledges CAPES/DAAD and PCI/CBPF for financial support.

- 
- [1] A. I. Buzdin, *Rev. Mod. Phys.* **77**, 935 (2005).  
 [2] M. Lange, M. J. V. Bael, A. V. Silhanek, and V. V. Moshchalkov, *Phys. Rev. B* **72**, 052507 (2005).  
 [3] M. J. Van Bael, K. Temst, V. V. Moshchalkov, and Y. Bruynseraede, *Phys. Rev. B* **59**, 14674 (1999).  
 [4] D. Aoki, A. Huxley, E. Ressouche, D. Braithwaite, J. Flouquet, J. Brison, E. Lhotel, and C. Paulsen, *Nature* **413**, 613 (2001).  
 [5] Z. Yang, M. Lange, A. Volodin, R. Szymczak, and V. V. Moshchalkov, *Nat. Mater.* **3**, 793 (2004).  
 [6] A. Palau, H. Parvaneh, N. A. Stelmashenko, H. Wang, J. L. Macmanus-Driscoll, and M. G. Blamire, *Phys. Rev. Lett.* **98**, 117003 (2007).  
 [7] S. Rubin, M. Holdenried, and H. Micklitz, *Eur. Phys. J. B* **5**, 23 (1998).  
 [8] A. Snezhko, T. Prozorov, and R. Prozorov, *Phys. Rev. B* **71**, 024527 (pages 6) (2005).  
 [9] T. H. Alden and J. D. Livingston, *J. Appl. Phys.* **37**, 3551 (1966).  
 [10] M. M. Doria, A. R. de C. Romaguera, M. V. Milosevic, and F. M. Peeters, *Eur. Phys. Lett.* **79**, 47006 (2007).  
 [11] M. M. Doria, *Physica C* **408**, 466 (2004).  
 [12] I. Sternfeld, V. Shelukhin, A. Tsukernik, M. Karpovskii, A. Gerber, and A. Palevski, *Phys. Rev. B* **71**, 064515 (2005).  
 [13] E. Wassermann, *Z. Physik* **187**, 369 (1965).  
 [14] Y. T. Xing, H. Micklitz, T. G. Rappoport, I. G. Solórzano-Naranjo, and E. Baggio-Saitovitch, to be submitted (2008).  
 [15] P. Santhanam, C. C. Chi, S. J. Wind, M. J. Brady, and J. J. Bucchignano, *Phys. Rev. Lett.* **66**, 2254 (1991).  
 [16] C. Strunk, V. Bruyndoncx, C. Van Haesendonck, V. V. Moshchalkov, Y. Bruynseraede, C.-J. Chien, B. Burk, and V. Chandrasekhar, *Phys. Rev. B* **57**, 10854 (1998).  
 [17] H. Vloeberghs, V. V. Moshchalkov, C. Van Haesendonck, R. Jonckheere, and Y. Bruynseraede, *Phys. Rev. Lett.* **69**, 1268 (1992).  
 [18] M. Park, M. S. Isaacson, and J. M. Parpia, *Phys. Rev. B* **55**, 9067 (1997).  
 [19] P. Lindqvist, A. Nordström, and O. Rapp, *Phys. Rev. Lett.* **64**, 2941 (1990).  
 [20] A. M. Petrean, L. M. Paulius, W.-K. Kwok, J. A. Fendrich, and G. W. Crabtree, *Phys. Rev. Lett.* **84**, 5852 (2000).  
 [21] N.-C. Yeh, D. S. Reed, W. Jiang, U. Kriplani, C. C. Tsuei, C. C. Chi, and F. Holtzberg, *Phys. Rev. Lett.* **71**, 4043 (1993).  
 [22] P. W. Anderson, *Phys. Rev. Lett.* **9**, 309 (1962).  
 [23] G. Blatter, M. V. Feigel'man, V. B. Geshkenbein, A. I. Larkin, and V. M. Vinokur, *Rev. Mod. Phys.* **66**, 1125 (1994).  
 [24] R. H. Koch, V. Foglietti, W. J. Gallagher, G. Koren, A. Gupta, and M. P. A. Fisher, *Phys. Rev. Lett.* **63**, 1511 (1989).  
 [25] W. Jiang, N.-C. Yeh, D. S. Reed, U. Kriplani, T. A. Tombrello, A. P. Rice, and F. Holtzberg, *Phys. Rev. B* **47**, 8308 (1993).  
 [26] N. D. Rizzo, J. Q. Wang, D. E. Prober, L. R. Motowidlo, and B. A. Zeitlin, *Appl. Phys. Lett.* **69**, 2285 (1996).  
 [27] G. Carneiro, *Phys. Rev. B* **69**, 214504 (pages 14) (2004).  
 [28] M. J. Van Bael, J. Bekaert, K. Temst, L. Van Look, V. V. Moshchalkov, Y. Bruynseraede, G. D. Howells, A. N. Grigorenko, S. J. Bending, and G. Borghs, *Phys. Rev. Lett.* **86**, 155 (2001).  
 [29] M. V. Milosevic, M. M. Doria, and F. M. Peeters, to be submitted (2008).